ACS APPLIED MATERIALS & INTERFACES

Research Article

www.acsami.org

Electrospun Superhydrophobic Membranes with Unique Structures for Membrane Distillation

Yuan Liao,[†,‡] Chun-Heng Loh,[‡] Rong Wang,*[,†,‡] and Anthony G. Fane[†,‡]

[†]School of Civil and Environmental Engineering, Nanyang Technological University, Singapore 639798, Singapore

[‡]Singapore Membrane Technology Centre, Nanyang Environment and Water Research Institute, Nanyang Technological University, Singapore 637141, Singapore

Supporting Information

ABSTRACT: With modest temperature demand, low operating pressure, and high solute rejection, membrane distillation (MD) is an attractive option for desalination, waste treatment, and food and pharmaceutical processing. However, large-scale practical applications of MD are still hindered by the absence of effective membranes with high hydrophobicity, high porosity, and adequate mechanical strength, which are important properties for MD permeation fluxes, stable long-term performance, and effective packing in modules without damage. This study describes novel design strategies for highly robust superhydrophobic dual-layer membranes for MD via electrospinning. One of the newly developed membranes comprises a durable and ultrathin 3-dimensional (3D) superhydrophobic skin and porous nanofibrous support whereas another was fabricated by electrospinning 3D superhydrophobic layers on a nonwoven support. These membranes exhibit superhydrophobicity toward distilled water, salty water, oil-in-water emulsion, and beverages, which enables them to be used not only for desalination but also for other processes. The superhydrophobic dual-layer membrane #3S-N with nanofibrous support has a competitive permeation flux of 24.6 ± 1.2 kg m^{-2} h^{-1} in MD (feed and permeate temperate were set as 333 and 293 K, respectively) due to the higher porosity of the nanofibrous scaffold. Meanwhile, the membranes with the nonwoven support exhibit greater mechanical strength due to this support combined with better long-term performance because of the thicker 3D superhydrophobic layers. The morphology, pore size, porosity, mechanical properties, and liquid enter pressure of water of these superhydrophobic composite membranes with two different structures are reported and compared with commercial polyvinylidene fluoride membranes.

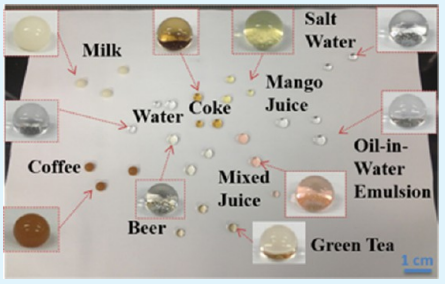

KEYWORDS: *dual-layer, three-dimensional, superhydrophobicity, membrane distillation, electrospinning*

1. INTRODUCTION

Different from other membrane processes that are isothermal and driven by transmembrane hydrostatic pressure, membrane distillation (MD) is a thermally driven process that has been studied for more than 40 years.[1,2] In the MD process, vapor is transported through a porous and hydrophobic membrane under a driving force of partial pressure gradient induced by the temperature difference between feed and permeate sides.[3−6] The membrane plays an essential role to hold the liquid/vapor interfaces at the entrance of the membrane pores, so that only vapor and noncondensable gases can pass through the pores. One of the advantages of MD over the conventional distillation process is that MD can readily be operated at modest temperatures, which, in turn, enable it to use waste heat and renewable energy sources.[7,8] Furthermore, due to theoretically complete rejection of ions, macromolecules, colloids, cells, and other nonvolatiles, MD processes have potential applications in manufacturing high-purity water, concentrating ionic, colloid, or other nonvolatile aqueous solutions.[9−11]

Although extensive research has been carried out on MD, it has had limited acceptance from a commercial stand point. Some of the barriers to commercialization of the MD process include membrane wetting over time, relatively low permeability, and the lack of rigid membranes for harsh operating conditions. To overcome these challenges, MD membranes need to be specially designed to exhibit high hydrophobicity, high porosity, good thermal stability, excellent chemical resistance, and mechanical rigidity to ensure higher permeation flux and better stability in long-term operation.[12]

To prepare highly hydrophobic membranes that can prevent wetting, the concept of superhydrophobicity has been considered. Inspired by the fascinating self-cleaning properties of the lotus leaf, silver ragwort leaf, and water strider leg in the natural world, these extremely water-repellent superhydrophobic surfaces have aroused great interest and been investigated due to potential applications in water harvesting, desalination, self-cleaning materials, antifogging surfaces, and so on.[13] Superhydrophobic surfaces, characterized by water contact angles of more than 150°, can be constructed by various approaches, including electrospinning, chemical modification, and sol−gel techniques.[13,14] Wang et al. has reviewed various investigations on modifying electrospun nanomaterials and

Received: June 20, 2014
Accepted: August 22, 2014
Published: August 22, 2014

direct electrospinning for rough superhydrophobic surfaces.[14] However, only a few studies have described efforts to fabricate superhydrophobic membranes for water desalination.[15−18] For example, superhydrophobic glass membranes with integrated arrays of nanospiked microchannels have been fabricated by several steps including glass fiber drawing, dissolving templates, chemical etching, and surface modifications.[15] However, the as-prepared superhydrophobic membranes prepared by this complex and tedious process had a low porosity of 26%, which decreased the mass transfer efficiency in MD. Previously, we have described surface modifications to alter polyvinylidene fluoride (PVDF) nanofiber membranes to be superhydrophobic with minor loss of MD flux and good nonwetting properties.[16] Although the superhydrophobic modified electrospun PVDF nanofiber membrane exhibited a promising MD flux attributed to the high porosity of the nanofibrous structure, the adhesion strength between the modification layers and the substrate maybe of limited duration. Superhydrophobic electrospun polystyrene (PS) micro/nanofibrous membranes with different thicknesses have been fabricated for the MD process, which also showed competitive permeation fluxes over 10 h of testing. However, the stability of the interface of the roughness-induced superhydrophobic surfaces, the thermal stability, chemical resistance, and mechanical rigidity of prepared PS membranes need to be further considered.

To further improve the wetting repellent property of superhydrophobic membranes, the development of three-dimensional (3D) superhydrophobic membranes is a possible solution. 3D superhydrophobic materials are distinct with maintenance of air at the surface as well as within the bulk of the materials, which can continuously provide a new water−air−material interface as water penetrates into it. Such materials have promising potential applications in the fields of chemical sensors, controlled release, and delivery and separation systems.[19−22] For example, tunable 3D porous superhydrophobic copper films with various wall thicknesses and pore sizes exhibiting integrated microstructures and nanostructures were synthesized by the gas bubble template-directed synthesis method.[22] 3D superhydrophobic dandelion-like microstructures were prepared by a self-assembly process from one-dimensional nanofibers, driven by a combined interaction of hydrogen bonding, $\pi-\pi$ stacking and hydrophobic interactions.[21] In addition, 3D superhydrophobic electrospun meshes have been fabricated as reinforcement materials for sustained local drug delivery against cancer cells, where air was used as a degradable component.[20] The infiltration of water into 3D superhydrophobic porous materials has been investigated in terms of, the boundary conditions at which superhydrophobicity can occur, the effects of addition of surfactant, the effects of solvents with various surface tensions, and the liquid entry pressure.[19]

However, 3D superhydrophobic membranes have not been designed or fabricated for the MD process. One limitation may be that, due to the large bulk porosity and surface porosity of the nanofibrous membrane, it may exhibit poor mechanical properties that have adverse impact on membrane assembly into the module. Some investigations have been carried out to enhance the mechanical properties of other MD membranes to satisfy the operational requirements. For example, clay particles have been added into the dope to improve the tensile modulus of PVDF hollow fibers fabricated for direct contact membrane distillation (DCMD).[23] Multibore PVDF hollow fiber membranes with a lotus root-like geometry have also been designed to optimize the mechanical rigidity and elasticity of the membranes.[24,25] However, no investigation has been reported to date to improve the mechanical properties of nanofiber MD membranes.

Therefore, in this work, we report two simple approaches to fabricate robust superhydrophobic dual-layer membranes with high porosity and excellent mechanical properties via electrospinning. The first approach involves electrospinning an ultrathin 3D superhydrophobic selective skin, comprising PVDF and silica nanoparticles, on a porous PVDF nanofibrous support. The second approach is to electrospin thicker 3D superhydrophobic PVDF−silica composite layers onto a commercial nonwoven support, which not only assists the PVDF−silica composite particles in shaping into a flat sheet but also provides outstanding mechanical properties to the composite membranes. The effects of dope compositions and membrane structures on water contact angle, water sliding angle, pore size and porosity, liquid entry pressure of water (LEPw), and mechanical properties of membranes were studied. MD tests were also carried out on selected membranes to examine their long-term performance. This study aims to compare the capabilities and performances of these two novel hierarchical-structure-designed membranes, and demonstrate that by carefully designing and manufacturing membranes to make them superhydrophobic and mechanically robust, the resultant membranes can achieve superior MD performance with high flux and long-term stability.

2. MATERIALS AND METHODS

2.1. Materials. Commercial polymer polyvinylidene fluoride (PVDF, Kynar HSV 900) was purchased from Arkema Inc., Singapore and was dried at 50 °C under vacuum before use. *N*,*N*-Dimethylformamide (DMF) and lithium chloride (LiCl) were provided by Merck, Singapore. Isopropyl alcohol (IPA) with analytical grade was obtained from VWR Co. Ltd., Singapore. Silica in spherical shape with particle size of 5−15 nm was purchased from Sigma-Aldrich, Singapore. To modify hydrophilic silica to be hydrophobic, α,ω-triethoxysilane-terminated perfluoropolyether ($(EtO)_3Si$-PFPE-$Si(OEt)_3$), with a trade name of Fluorolink S10 (FS10), was obtained from Solvay Solexis. Tetraethoxysilane (TEOS) (Merck, Singapore) and *n*-hexane (Merck, Singapore) were used as cross-linking agent and solvent, respectively, in silica modification. All reagents were used as received. Water was purified with a Milli-Q system (Millipore Co., Singapore). Commercial PVDF membranes, Durapore membrane filter GVHP, were purchased from Millipore, Singapore for comparison with the composite PVDF membranes prepared in this study. Polyethylene terephthalate (PET) nonwoven scaffolds (Hollytex 3233) were purchased from Ahlstrom Filtration, USA.

2.2. Fabrication of Superhydrophobic Dual-Layer Membranes by Electrospinning. To stabilize the PVDF−silica composite and achieve a good dispersion of silica particles in the PVDF dope, the purchased silica needed to be modified with the hydrophobic reagent FS10. Briefly, a desired amount of silica was stirred rapidly overnight in *n*-hexane solution in which FS10 and TEOS with a mass ratio of 3:2 was added. The modified silica particles were then separated by centrifugation and annealed in the vacuum oven at 100 °C for 1 h. The as-prepared FS10-modified silica was then added into different PVDF dope solutions, which were subsequently used to fabricate the superhydrophobic selective layer of the membranes by electrospinning.[2]

The electrospinning parameters for the various membranes prepared are summarized in Table 1. For the electrospinning of dual-layer membranes with nanofibrous support, a porous support layer was first fabricated using an 8 wt % PVDF dope. A desired amount of LiCl (0.004 wt %) was added into the dope solution to improve the dope electrospinning ability, optimize the nanofiber membrane porosity, and control membrane pore size.[2] On top of the

Table 1. Operating Parameters for Preparing Superhydrophobic Nanofiber Membranes

membrane ID	#3S-N	#4S-N	#5S-N	#4S-W	#5S-W
dope composition of selective layer (wt %)	PVDF/SiO_2/DMF:3/6/97	PVDF/SiO_2/DMF:4/8/96	PVDF/SiO_2/DMF:5/10/95	PVDF/SiO_2/DMF:4/8/96	PVDF/SiO_2/DMF:5/10/95
dope composition of support layer (wt %)	PVDF/DMF: 8/92 (0.04 wt % LiCl as additive)			nonwoven scaffold	
dope flow rate (selective/support layer)(mL min^{-1})	0.02/0.03			0.03/–	
travel speed (mm sec^{-1})	0.1				
travel distance (cm)	7				
distance (cm)	12				
voltage (selective/support layer) (kV)	28/26			28/–	
loop number (selective/support layer)	6/15	6/15	6/15	20/–	

electrospun PVDF support layer, a thin selective layer was electrospun using various PVDF dopes blended with hydrophobic-modified silica. The concentration of PVDF dopes varied from 3 to 5 wt % while the mass ratio of silica to PVDF was kept constant at 2:1. The as-prepared dual-layer membranes were coded as #3S-N, #4S-N, and #5S-N, respectively. Another type of superhydrophobic dual-layer membranes #4S-W and #5S-W was prepared by electrospinning PVDF−silica dopes onto a nonwoven support, as shown in Table 1. All fabricated membranes had a thickness of 72 ± 12 μm. (For the membranes with nonwoven supports, the thickness of the nonwoven supports were excluded from the measurement.)

2.3. Characterization of PVDF Nanofibrous and Composite Membranes. X-ray photoelectron spectroscopy (XPS) was conducted using a Theta Probe XPS (Thermo Fisher Scientific, Singapore) to analyze the chemical composition on the membrane surface. The surface morphology of the resultant membranes was observed by a field emission scanning electron microscopy (FE-SEM, JSM-7600F, JEOL Asia Pte Ltd., Japan) instrument, which is equipped with an energy-dispersive X-ray spectroscopy (EDX) detector. The accelerating voltages applied for FE-SEM observation and FE-SEM-EDX measurements were set as 5 and 10 kV, respectively. The topography of the superhydrophobic composite membranes surfaces were characterized by means of an atomic force microscopy (AFM, XE-100, Park Systems, Korea). An area of 2.5 × 2.5 μm was scanned using the tapping mode, which was operated in air at 26 °C. Three replicate experiments were conducted.

The water contact angles of fabricated membranes were measured by a goniometer (Contact Angle System OCA, Data Physics Instruments GmbH, Singapore). Water sliding angles were also determined by placing a 10 μL water droplet on a horizontal membrane surface, as shown in Figure S1 (Supporting Information), followed by gradually tilting the membrane until the water droplet started to roll off from the surface.

The pore sizes of the as-prepared membranes were determined by a capillary flow porometer (CFP 1500A, Porous Materials, Inc. (PMI), Singapore). Liquid enter pressures of water (LEPw) of the membranes were measured in a dead-end cell using Milli-Q water, as shown in Figure S2 (Supporting Information). The pressure on the membrane was increased stepwise while allowing a stabilization time of 10 min after each 14 kPa (2 psi) increment. The pressure at which the first drop of permeate was observed was recorded as the LEPw. The membrane porosity is defined as the volume of the pores divided by the total volume of the membrane, and was determined by the gravimetric method (described in the Supporting Information). The mechanical properties of the membranes were measured using a Zwick/Roell BT1-FR0.5TN.D14 testing machine at a constant elongation velocity of 50 mm min^{-1} at room temperature (26 °C). The stability of modified silica was examined by eroding composite membranes surface using 2 L NaCl solution with a concentration of 3.5 wt % and a flow rate of 0.6 L min^{-1} for 24 h. The silica concentrations of original and tested salt solutions were determined by an inductively coupled plasma optical emission spectrometry (ICP, Optima 8000, PerkinElmer, USA), which was calibrated using 1, 3, and 5 ppm of Si standard solutions (Inorganic Ventures, Singapore).

2.4. MD Performance Test. The MD performance of selected PVDF composite membranes was tested in a DCMD setup with an effective membrane area of 38 cm^2. The configuration of this DCMD setup has been detailed in our previous work.[2] Both the feed and permeate solutions were circulated through the flat-sheet membrane cell. The feed solution, with 3.5 wt % sodium chloride, was heated to 333 K and circulated with a flow rate of 0.6 L min^{-1}. The permeate solution, which was Milli-Q water with a conductivity below 5 μs cm^{-1}, was cooled down to 293 K and circulated by a peristaltic pump at the same flow rate. The permeate flux was collected in an overflow tank placed on a digital balance. Over the duration of the MD experiment, the membrane cell and connecting tubes were insulated to prevent heat loss. The experimental data were recorded by a data-logging system in real time.

3. RESULTS AND DISCUSSION

3.1. Effects of Silica Modification and Dope Concentration on Stability of Dispersion. When silica−polymer composites are prepared, the interfacial interaction between the phases of silica and polymer is a decisive factor affecting the properties of the resulting materials.[26] As shown in Figure S3A (Supporting Information), the hydrogen bonds on the silica surface can be sufficiently strong such that the formed aggregates remain intact even under vigorous mixing, which, in turn, has a significant impact on the prepared membranes.[27] Nanosilica possesses a three-dimensional network, the surface of which is typically terminated with free or isolated silanols, hydrogen-bonded or vicinal silanols, and germinal silanols.[28] These silanol groups residing on adjacent silica particles tend to form hydrogen bonds and lead to agglomerates of silica in the polymer matrix. An effective dispersion to break down nanoparticles agglomeration could be achieved by hydrophobic modification of the hydrophilic silica surface, as shown in Figure S3B (Supporting Information). By doing so, it is postulated that the hydrophobic fluoride chains on the modified silica surface could exhibit better compatibility with PVDF, thus improving the dispersion of nanosilica in the polymer matrix.

To modify the silica nanoparticles to become hydrophobic, an attempt to graft FS10 onto the silica surface was carried out by alcohol condensation reactions between the hydroxyl groups of TEOS and silanol groups of silica particles or FS10. The possible reaction mechanism is shown in Figure S4 (Supporting Information). Figure 1 shows the XPS spectra of unmodified silica (SiO_2) and FS10-grafted silica (FS-SiO_2). From the XPS spectra, compared with silica nanoparticles only possessing silicon and oxygen elements on their surfaces, the FS-SiO_2 shows additional carbon, nitrogen, and fluorine peaks. These additional elements are in accordance with the chemical structure of FS10, suggesting that the hydrophobic FS10 has been successfully grafted onto the silica surface.[29] In addition, a significant reduction in the intensity of the silica peak can also be observed after the modification, indicating that the FS-SiO_2 has a strong surface enrichment of organic phase such as carbon and fluoride after the modification reaction by the hydrophobic FS10. Due to the hydrophobic nature of FS-SiO_2, via grafting polymerization, nanoparticles agglomerates are altered into a nanocomposite microstructure, which can build up a stronger interfacial interaction with the surrounding PVDF chains. This in turn prevents agglomerates and facilitates a better dispersion when mixing FS-SiO_2 with PVDF, as shown in Figure S3B (Supporting Information).

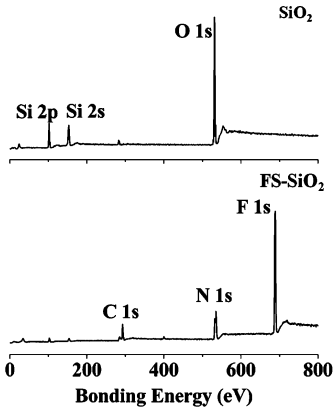

Figure 1. XPS wide-scan spectra of pristine silica and modified silica nanoparticles (FS-SiO_2).

Moreover, the stability of FS-SiO_2−PVDF dispersion is significant for fabricating nanocomposite membranes by electrospinning, as the dopes need to be homogeneous during spinning. To observe the stability of the dispersion, FS-SiO_2-blended PVDF dopes with varied PVDF concentrations (mass ratio of FS-SiO_2 to PVDF was fixed at 2:1) were left to stand for several hours. The images of as prepared PVDF dopes after standing for different durations are shown in Figure 2A. At the beginning, all the dopes were homogeneous. However, the dope with 2 wt % PVDF had separated into two phases after 30 min. After 4 h, the dope with 3 wt % PVDF was also observed to be separated. These observations suggest that homogeneous dispersion lasts for a longer time in a more concentrated dope. This might be due to a better entanglement between PVDF macromolecular chains and FS-SiO_2 particles, which prevents the particles from settling fast, when the dope is more concentrated (Figure 2B,C).

Considering that the electrospinning of the superhydrophobic dual-layer membrane with nonwoven support would take roughly 4 h, the dopes containing 4 and 5 wt % PVDF were selected for the membrane preparation because they represent excellent stability after standing for 4 h. For the case of the superhydrophobic dual-layer membrane with nanofibrous support, the electrospinning of superhydrophobic selective layer could be completed within 1 h. Thus, the dope containing 3 wt % PVDF could also be utilized to prepare the membranes.

Table 2 summarizes the chemical compositions of the pristine PVDF nanofibrous membrane, FS-SiO_2, and FS-SiO_2-blended PVDF composite membrane surfaces. The C/F ratio of the PVDF nanofibrous membrane is 1.0, which shows consistency with the theoretical ratio of PVDF. The FS-SiO_2 exhibits lower C/F ratio of 0.7 due to the higher content of fluoride in the modifier FS10. Meanwhile, the C/F ratio on the FS-SiO_2-blended PVDF composite membrane surface is 0.9, which suggests that the composite membrane surface contains a great amount of PVDF materials.[30]

3.2. Morphology of FS-SiO_2−PVDF Composite Membranes. Figure 3 shows the diagrams, surfaces, cross-sectional morphologies, and EDX mappings of superhydrophobic dual-layer composite membranes with nanofiber and nonwoven supports. According to the designed hierarchical structure of the composite membrane with nanofibrous support as shown in Figure 3A1, the membrane constitutes a porous PVDF nanofibrous support layer with nanofiber diameter of 180 ± 3 nm (Figure 3A2), and a FS-SiO_2−PVDF superhydrophobic selective layer with a thickness of 12 ± 2 μm (Figure 3A3). The cross section of this superhydrophobic dual-layer membrane is shown in Figure 3A4. The surface morphology of the membrane with nanofibrous support shows a structure with large amounts of protrusions and valleys, which provide microscaled and nanoscaled roughness for superhydrophobicity. As shown in Figure 3B1, this superhydrophobic dual-layer membrane comprises a nonwoven scaffold and a FS-SiO_2−PVDF composite layer (Figure 3B2). In Figure 3B3, the surface morphology of the membrane with nonwoven support is observed to be similar to that with nanofibrous support. The cross sectional morphology of the membrane is comprised of microbeads and nanobeads (Figure 3B4). These micro- and nanobeads, which are formed due to the presence of the FS-SiO_2 particles, make up the majority of the cross section and

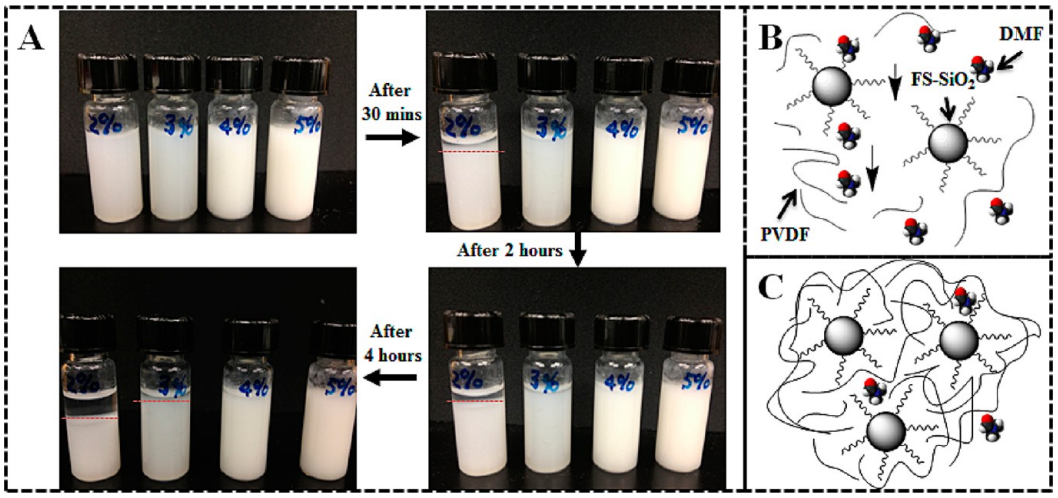

Figure 2. (A) Photographs of various FS-SiO_2-blended PVDF dopes after hours and schematic illustrations of (B) unstable low concentration dope and (C) stable high concentration dope.

Table 2. Element Concentration of the PVDF Nanofibrous Membrane, FS-SiO_2, and FS-SiO_2-blended PVDF Composite Membrane

atomic conc. (%)[a]	PVDF (theoretical)	PVDF nanofibrous membrane	FS-SiO_2	FS-SiO_2-blended PVDF composite membrane
C	50.0	51.0	29.4	37.7
F	50.0	49.0	42.4	41.2
C/F	1.0	1.0	0.7	0.9

[a]Determined from the corrected C 1s and F 1s XPS core-level spectra area ratio of the respective sample.

thus form a thicker "three-dimensional roughness". This unique structure plays an important role in long-term performance of MD, as will be discussed in a later section

It is worth pointing out that in order to improve the integrity of both composite membranes, it is necessary to ensure strong adhesion at the interface between the composite skin layer and the nanofibrous support, and also guarantee robust connection between the composite layer and nonwoven scaffold. Therefore, an additive, such as LiCl, was not added into the composite FS-SiO_2–PVDF dopes because the presence of such additive would reduce the fiber diameter, increase the length–diameter ratio, and consequently accelerate the evaporation of solvent during electrospinning.[31] If the solvent evaporation is fast, such that beads and fibers become completely dry when they are deposited on the support, poor adhesion between the composite layer and nanofibrous support or PET nonwoven support is likely to occur. In such case, the resultant membranes might not be robust enough to withstand changes in flow velocity and other stresses.[31] In contrast, in the case of fabricating highly porous nanofibrous supports, an inorganic additive, LiCl, is necessary to accelerate solvent evaporation, fabricate dry nanofibers and get porous nanofibrous membranes. In this way, the dry nanofibers cannot be adhered to the PET nonwoven scaffold. To demonstrate the strong adhesion between composite layers and nanofibrious or nonwoven supports, the magnified images and EDX mappings of cross sections of nanofiber-supported and nonwoven-supported membranes are shown in Figure 3C,D, respectively. According to Figure 3C1, no delamination between the nanofibrous support layer and the selective layer is observed, confirming a good adhesion at the interface. To further present the interact boundary between PVDF nanofibers and composite layers, the EDX mappings of amplified membrane cross-section are shown from Figure 3C2–4. The silica element was only distributed on the surface skin layer while the fluoride was distributed uniformly in the bulk membrane. No delamination was shown in the boundary line. Figure 3D shows the cross section of nonwoven-supported composite membrane in higher magnification and EDX mappings around one PET nonwoven fiber, which proves that the composite materials intruded and wrapped the nonwoven fibers and thus confirms the strong adhesive force between them.

3.3. Superhydrophobicity of FS-SiO_2–PVDF Composite Membranes. The variations of water contact angle and sliding angle of different membranes are shown in Figure 4. Compared with the commercial PVDF membrane GVHP possessing a contact angle of 135° ± 6°, all as-prepared membranes show a higher water contact angle of more than 150°, indicating that these membranes are superhydrophobic. In addition, water droplets tend to adhere on the surface of the commercial PVDF membrane even after turning the membrane upside down, as shown in Figure 4. In contrast, all as-prepared superhydrophobic membranes exhibit a water sliding angle lower than 30°.

As further evidence for the superhydrophobicity, Figure 5A shows how a water droplet on a needle tip interacted with the surface of a superhydrophobic membrane when the needle was brought near to and away from the membrane. The water droplet did not show any tendency to spread on the superhydrophobic surface of the as-prepared membranes even when the water droplet on membrane surface was pushed by the needle. The membrane surface remained dry after moving the needle away from the surface. A key membrane characteristic responsible for the superhydrophobicity is the surface topography. Therefore, the surface topography of as-prepared superhydrophobic membranes was examined by AFM. As shown in Figure 5B, the membrane surface shows a structure with ridges and valleys, which are attributed to the formation of micro- and nanobeads comprising the FS-SiO_2–PVDF composite. The FS-SiO_2–PVDF composite has small asperities scattered on the membrane surface, which are essential to enhance the roughness and achieve super-

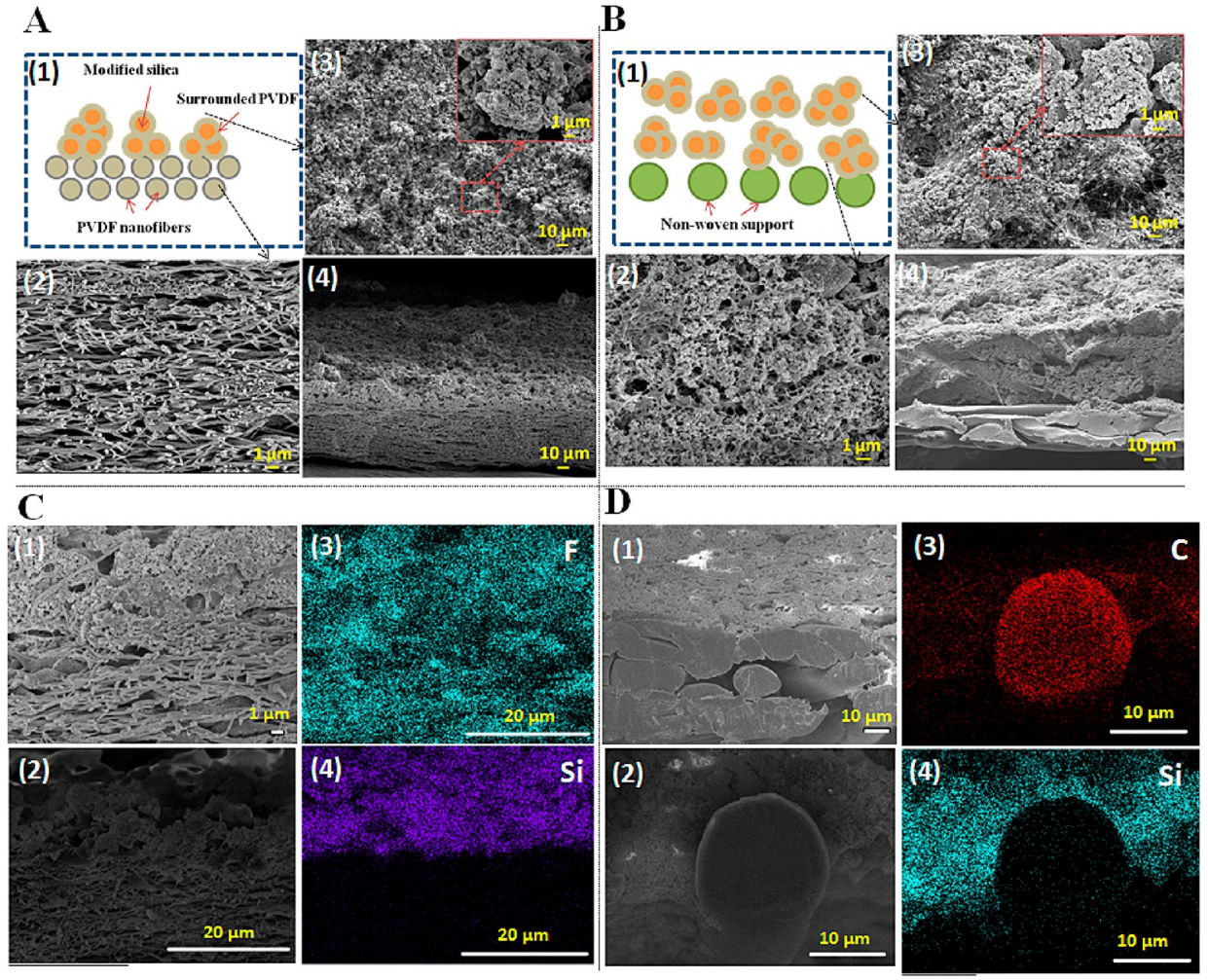

Figure 3. Diagrams and morphologies of superhydrophobic dual-layer membranes (A) #3S-N and (B) #5S-W: (1) schematic drawing; (2) enlarged cross section image of the middle layer; (3) surface morphology; (4) cross section morphology of prepared membranes. (C): (1) Enlarged interacting morphology image between FS-SiO_2-blended PVDF composite and PVDF nanofibrious layers of #3S-N; (2–4) the EDX mapping of the #3S-N cross section showing the distribution of F and Si elements. (D): (1) Enlarged interacting morphology image between FS-SiO_2-blended PVDF composite and PET nonwoven layers of #5S-W; (2–4) the EDX mapping of the #5S-W cross section showing the distribution of C and Si elements.

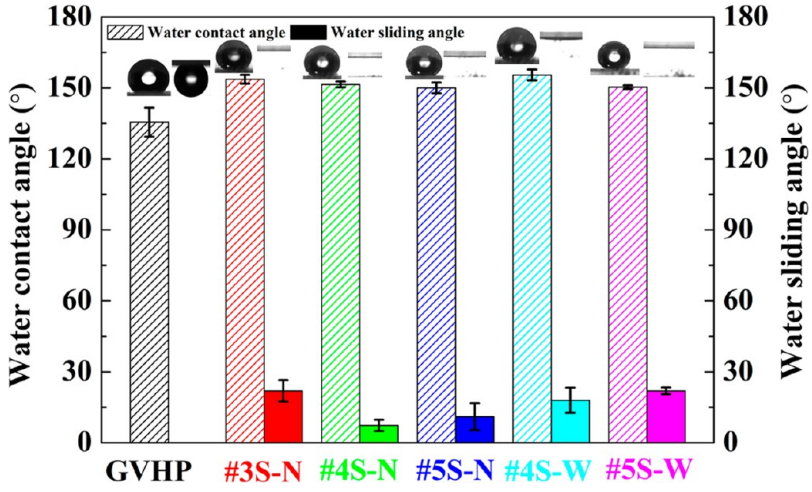

Figure 4. Variations of water contact angle and sliding angles as a function of different membranes fabrication dopes and structures.

dx.doi.org/10.1021/am503968n | *ACS Appl. Mater. Interfaces* 2014, 6, 16035–16048

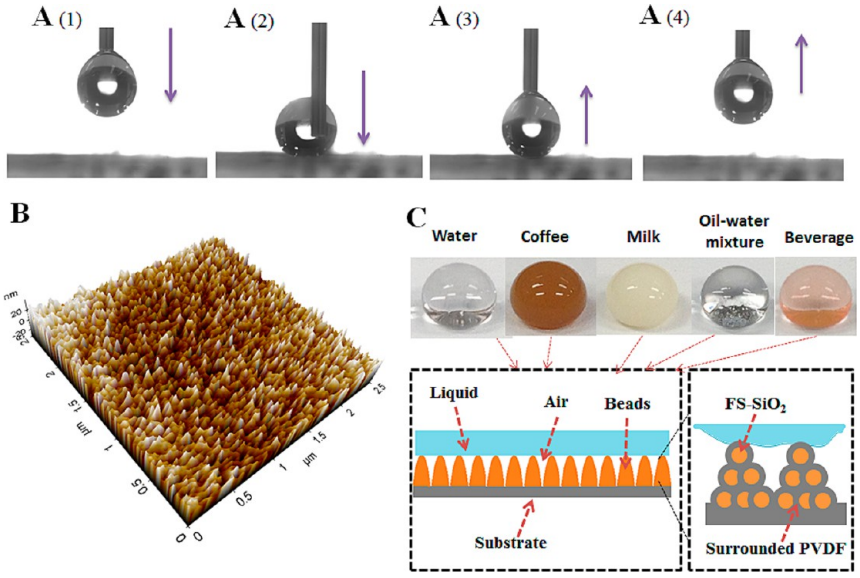

Figure 5. (A) Captured images of water droplet movement on the surface of superhydrophobic membrane #3S-N, (B) surface topography of superhydrophobic membrane #3S-N, and (C) the liquid–membrane interface scheme on silica blended superhydrophobic membrane.

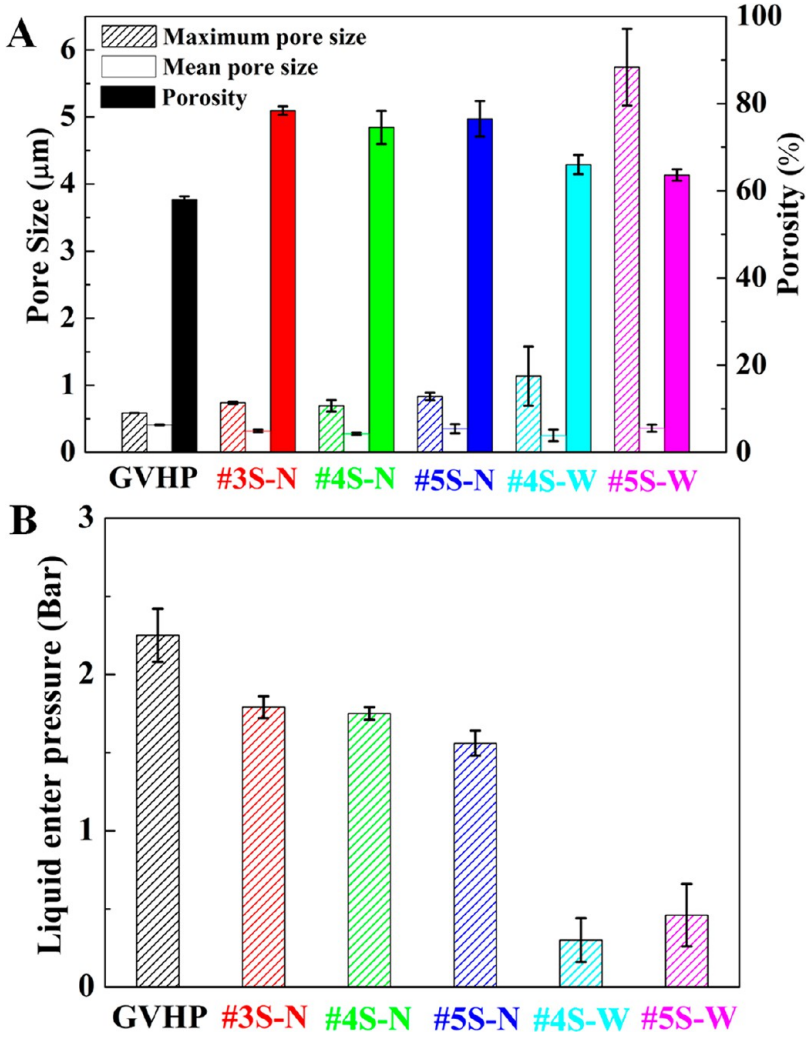

Figure 6. Comparisons of (A) pore sizes and porosity, and (B) LEPw of different PVDF membranes.

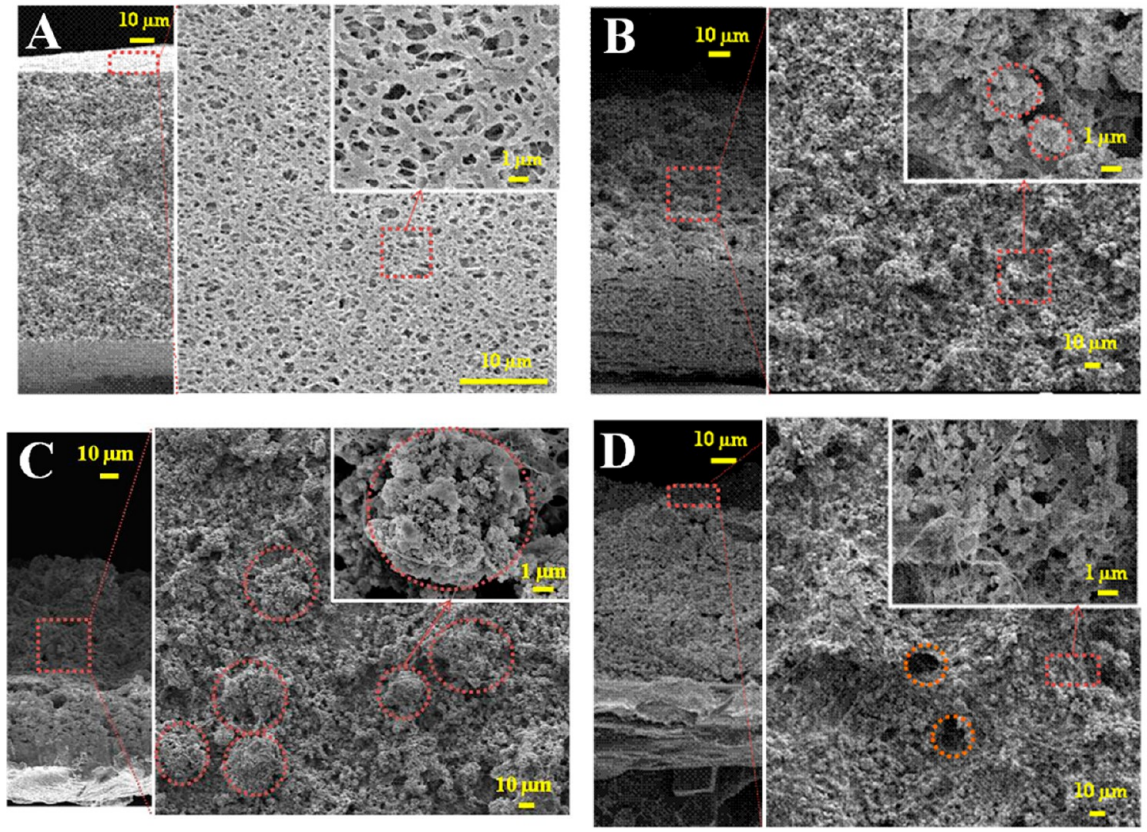

Figure 7. Cross section and surface morphologies of commercial PVDF membrane GVHP (A), #3S-N (B), #4S-N (C), and #5S-W (D).

hydrophobicity. The contact angle of a liquid on such a rough surface comprising solid (the ridges) and void (the valleys) can be described by the Cassie–Baxter equation:[32]

$$\cos\theta_r = f_{ls}\cos\theta_0 - f_{lv} \quad (1)$$

where θ_r is the observed contact angle of a liquid on a rough surface (deg), θ_0 is the intrinsic contact angle of the liquid on corresponding smooth surface (deg), f_{ls} is the ratio of the liquid–solid contact area to the total projected area, and f_{lv} is the areal fraction of the void. As illustrated in Figure 5C, air is trapped under the liquid droplet between the small peaks shaped by silica–PVDF composites, which implies an increase of f_{lv} and therefore superhydrophobicity. The liquid droplet is suspended on the top of the asperities and the air fraction present between the surface and liquid droplet makes its suspension much easier, which consequently enables the liquid to roll off the membrane surface spontaneously after tilting to a small angle. For such a surface, the term "self-cleaning" has been introduced.[33] Due to the nanorough surface, the as-prepared membranes exhibit superhydrophobicity to not only water but also other liquids such as coffee, milk, oil-in-water emulsion (1 wt % silica oil in water), and beverage, as shown in Figure 5C.

3.4. Comparison of Different PVDF Membranes. The pore size and porosity of commercial PVDF and fabricated superhydrophobic PVDF membranes as well as their LEPw are summarized in Figure 6. The pore size distributions of these membranes are shown in Figure S5 (Supporting Information). Compared with the membranes fabricated in this work, because of the sponge-like structure as shown in Figure 7A, the commercial PVDF membrane possesses the smallest maximum and mean pore sizes, which are 0.59 ± 0.01 and 0.41 ± 0.01 μm, respectively. For the superhydrophobic dual-layer membranes with nanofibrous support, it is found that the maximum pore size of #5S-N (0.83 ± 0.06 μm) is larger than that of #3S-N and #4S-N, indicating that the pore size tends to increase when the dope was prepared with a higher concentration of PVDF and FS-SiO_2. This might be attributed to the formation of larger beads with increasing dope concentration, as shown in Figure 7B,C. The larger beads tend to exhibit a higher accumulated charge during electrospinning, thus creating a stronger repulsive force between each other. As a result, the membrane prepared using a dope with a higher concentration (i.e., #5S-N) exhibits a less compact structure and a larger pore size.

On the other hand, the maximum pore size of the superhydrophobic dual-layer membrane with nonwoven support #5S-W (>5.5 μm) is observed to be significantly larger than all the other membranes. This make the membrane unsuitable for MD application because maximum pore sizes of most MD membranes are below 0.6 μm.[34] Compared with the dual-layer membranes with nanofibrous scaffold, it seems that the dope composition has a more significant effect on pore size for membranes prepared mainly by PVDF and FS-SiO_2 composite dope. This might be because, unlike the membranes that consist of a thin layer of bead structure (the selective layer) and a bulk structure composed of overlapped nanofibers, the majority of the membranes with nonwoven support are made up of micro- and nanobeads (as described in section 3.2). Due to the repulsive forces between the beads during electrospinning as mentioned above, it is possible to produce even larger holes on the surface, as shown in Figure 7D. As a result, the maximum pore size of the nonwoven-supported membranes is increased.

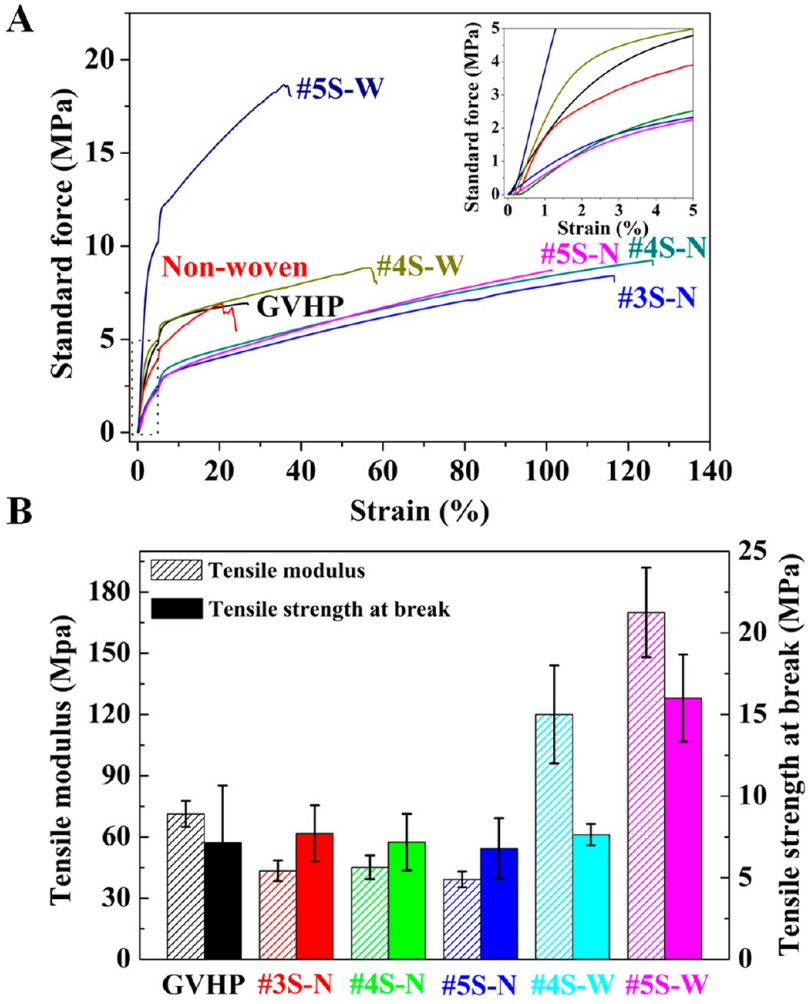

Figure 8. (A) Stress–strain curves at ambient temperature and (B) tensile modulus and tensile strength at break of commercial and as-fabricated PVDF composite membranes.

The overall porosity of the PVDF membranes is also presented in Figure 6A. It is observed that the commercial PVDF membrane has the lowest porosity of 58 ± 1% compared with the as-prepared membranes. In general, the nonwoven-supported membranes exhibit a lower porosity than the nanofiber-supported membranes due to their much more compact structure. Thanks to the porous nanofibrous support of the dual-layer membranes #3S-N, #4S-N, and #5S-N, they all exhibit a higher porosity around 80%, which could decrease the mass transfer resistance in the MD process.

As noted above, one of the critical membrane characteristics for MD application is the stability of membrane performance in long-term usage, which could be related to the liquid entry pressure of water (LEPw). When the hydraulic pressure on the membrane surface exceeds LEPw, water and salt in the feed side will overcome the surface tension and enter the hydrophobic membrane pores. This contaminates the permeate and reduces the flux significantly. According to the Laplace equation, the LEPw is directly proportional to the cosine of liquid–solid contact angle (θ), the liquid surface tension (γ_L), and the geometric factor (B), and is inversely proportional to the largest pore radius (r_{max}) as follows:[35]

$$P_{liquid} - P_{vapor} = \Delta P_{interface} = \frac{-2\gamma_L B\cos\theta}{r_{max}} < \text{LEPw} \quad (2)$$

A reduction of r_{max} and an enhancement of θ would increase the LEPw of a membrane. As can be seen in Figure 6B, the commercial membrane exhibits the largest LEPw of 2.25 ± 0.17 bar due to its smallest pore size. Although the nanofiber-supported dual-layer membranes have a larger pore size and a higher porosity, they still show competitive LEPw values above 1.5 bar. This is attributed to the enhanced contact angle due to the rough surface. On the other hand, the LEPw of the dual-layer superhydrophobic membranes with nonwoven support are around 0.5 bar because of the presence of big pores. However, this did not appear to compromise its long-term performance (see in section 3.5).

The tensile stress–strain curves of commercial and electrospun PVDF membranes are shown in Figure 8A. Mechanical reinforcement can be achieved when the nanofiber and nanobeads are dispersed and attached on the nonwoven support such that the external load is efficiently transferred between the composite layer and the nonwoven support layer. When the stress–strain curves for the nonwoven-supported superhydrophobic membranes are compared with that of the nanofiber-supported and commercial membranes, it is clear that the tensile modulus (slope of the initial, linear portion of stress–strain curve) of nonwoven-supported membranes is improved. In addition, because of the excellent combination between the composite layer and the nonwoven support layer,

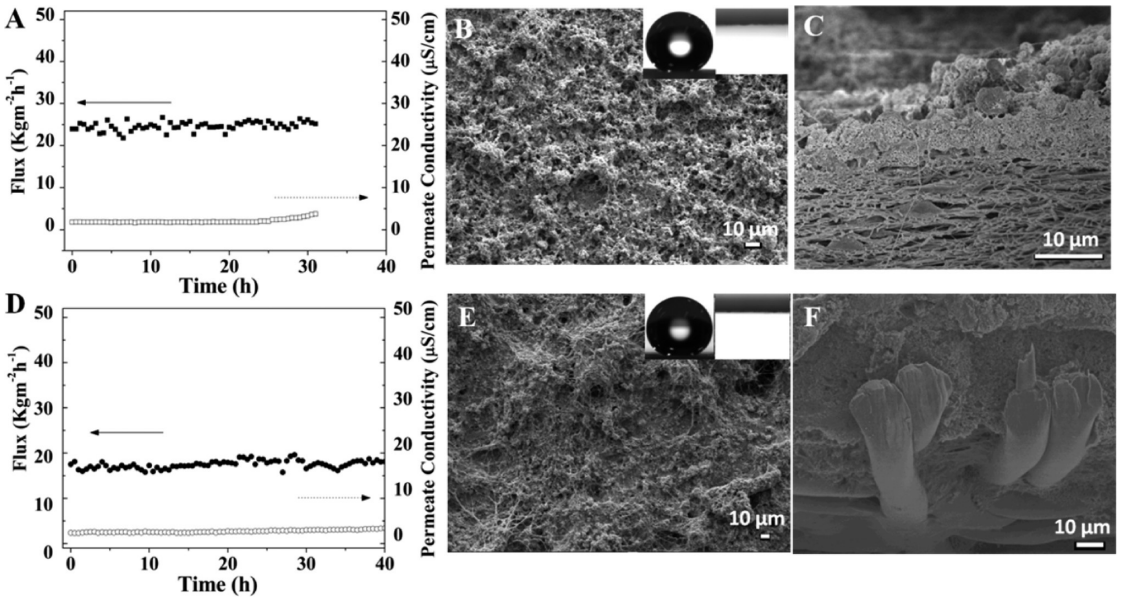

Figure 9. Continuous DCMD test, membrane surface, and cross-sectional morphology after the test of #3S-N (A, B, and C) and #5S-W superhydrophobic membranes (D, E, and F). (3.5 wt % NaCl solution as feed, T_f = 333 K, T_p = 293 K).

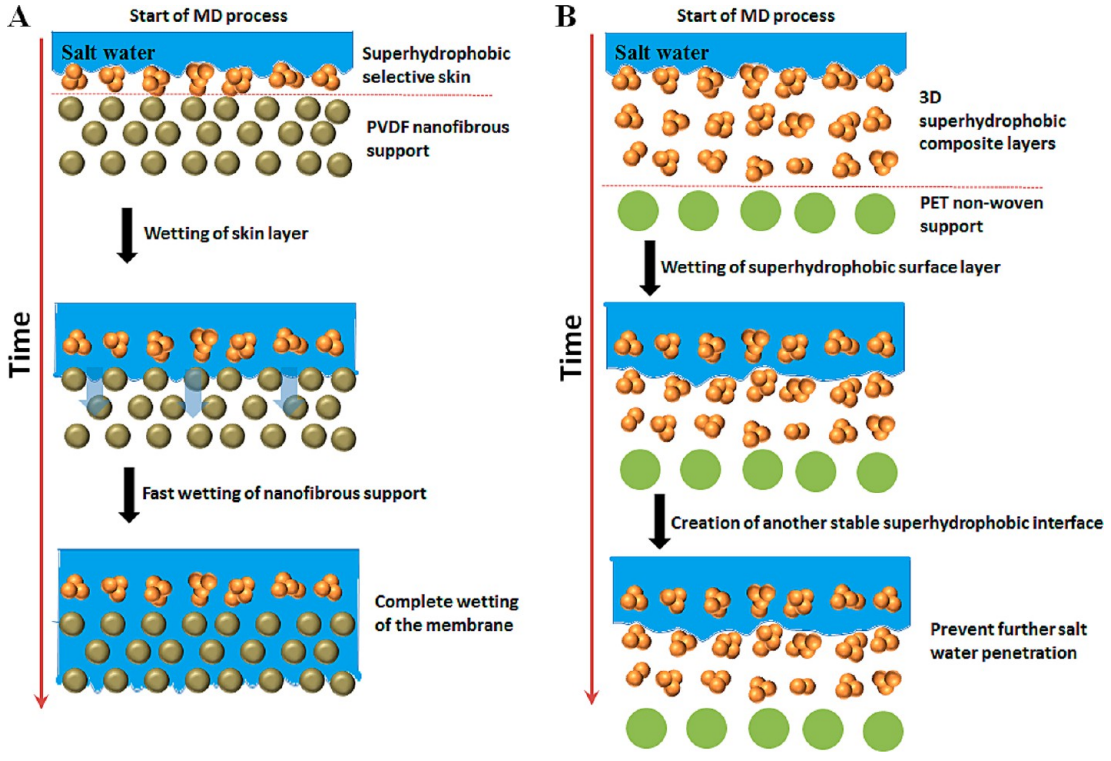

Figure 10. Comparison between the behavior of superhydrophobic membranes (A) #3S-N and (B) #5S-W in continuous MD process. Once the metastable superhydrophobic #3S-N loses the air entrapped at the interface, the salt water tends to penetrate in nanofibrous layer relatively quickly until complete wetting of the membrane. In comparison, the 3D superhydrophobic composite membrane #5S-W could create a new superhydrophobic water−air−material interface after losing the upmost superhydrophobic layer.

the prepared membranes possess better mechanical strength than the nonwoven scaffold itself. The average tensile modulus and the ultimate tensile strength of the membranes are summarized in Figure 8B. The tensile modulus of #5S-W (170 ± 22 MPa) increased by 336% compared with the dual-layer membrane #5S-N (39 ± 4 MPa). Moreover, the tensile strengths of the dual-layer membranes with nonwoven support are also better than those with nanofibrous support.

3.5. Continuous DCMD Performance. The newly developed superhydrophobic membranes #3S-N and #5S-W were chosen to test in the DCMD process, as #3S-N possesses the highest porosity and #5S-W exhibits the best mechanical properties. Before utilizing these composite membranes in DCMD, the contact angles of water were measured at elevated temperatures from 60 to 80 °C, which are the operational temperatures for MD application. Figure S6A,B (Supporting

Table 3. Properties and DCMD Performance of Different Electrospun PVDF Nanofiber Membranes

membrane		mean pore size (μm)	max pore size (μm)	membrane thickness (μm)	contact angle (deg)	Young's modulus (Mpa)	tensile strength (Mpa)	elongation at break (%)	feed solution property: solution	feed solution property: $T_{f,in}$ (°C)	permeate solution property: solution	permeate solution property: $T_{p,in}$ (°C)	permeation flux (kg m^2 h^{-1})	rejection (%)	long-term performance
PVDF–clay nanofiber membranes[37]	S1	0.58	–[a]	–[a]	128	–[a]	–[a]	–[a]	3.5 wt % NaCl	80	–[a]	17	6[b]	98.27	wet in 8 h
	S2	0.60	–[a]	–[a]	134	–[a]	–[a]	–[a]	3.5 wt % NaCl	80	–[a]	17	6[b]	99.95	wet in 8 h
	S3	0.63	–[a]	–[a]	142	–[a]	–[a]	–[a]	3.5 wt % NaCl	80	–[a]	17	5[b]	99.99	stable in 8 h
	S4	0.64	–[a]	–[a]	154	–[a]	–[a]	–[a]	3.5 wt % NaCl	80	–[a]	17	5[b]	99.97	stable in 8 h
PVDF–HFP nanofiber membrane[38]	10 PH-hot pressed 2 layer	0.26	0.77	110	–[a]	–[a]	–[a]	–[a]	1.0 wt % NaCl (18 mS cm^{-1})	65	tap water (110 μS cm^{-1})	24	20–21	98[d]	–[a]
	15 PH-hot pressed 2 layer	0.51	1.04	170	–[a]	–[a]	–[a]	–[a]	1.0 wt % NaCl (18 mS cm^{-1})	50	tap water (110 μS cm^{-1})	24	8–9	98[d]	–[a]
PVDF nanofiber membrane[39]	EMN 1 h	–[a]	5.20[b,c]	144	139	24	4.5	138	3.0 wt % NaCl	60	distilled water	20	28[b]	99.4[e]	the change of permeation flux and conductivity was below 5% in 25 h
	EMN 2 h	–[a]	4.40[b,c]	464	139	35	6.4	134	3.0 wt % NaCl	60	distilled water	20	13[b]	99.9[e]	
	EMN 3 h	–[a]	3.80[b,c]	833	140	44	7.2	134	3.0 wt % NaCl	60	distilled water	20	11[b]	99.9[e]	
	EMN 4 h	–[a]	2.90[b,c]	1529	139	75	10.2	130	3.0 wt % NaCl	60	distilled water	20	7[b]	99.9[e]	
PVDF nanofiber membrane[2]	M-9-LS-LM-heat	0.18	0.36	–[a]	138	–[a]	–[a]	–[a]	3.5 wt % NaCl (60 mS cm^{-1})	60	distilled water (<5 μS cm^{-1})	20	11	>99.99[e]	stable in 10 h
	M-9-LS-LM-heat	0.21	0.33	–[a]	136	–[a]	–[a]	–[a]	3.5 wt % NaCl (60 mS cm^{-1})	60	distilled water (<5 μS cm^{-1})	20	21	>99.99[e]	stable in 15 h
This Work	#3S-N	0.32	0.74	72	154	68	7.9	94	3.5 wt % NaCl (60 mS cm^{-1})	60	distilled water (<5 μS cm^{-1})	20	25	>99.99[e]	stable in 25 h
	#5S-W	0.36	5.74	76	150	369	16.9	34	3.5 wt % NaCl (60 mS cm^{-1})	60	distilled water (<5 μS cm^{-1})	20	21	>99.99[e]	stable in 40 h

[a]The data were not shown in the paper. [b]The data were taken from figures shown in papers. [c]Interfiber space. [d]The rejection %SR was caculated by the following equation, where C_{feed}, $C_{permeate}$, and $C_{tapwater}$ are the conductivity of feed, permeate, and tapwater, respectively.

$$\%SR = \frac{C_{feed} - (C_{permeate} - C_{tapwater})}{C_{feed}} \times 100\%$$

[e]The rejection η was caculated by following equation, where $C_{b,f}$ and $C_{b,p}$ are the conductivity of feed and permeation, respectively.

$$\eta = (1 - C_{b,p}/C_{b,f}) \times 100\%$$

dx.doi.org/10.1021/am503968n | ACS Appl. Mater. Interfaces 2014, 6, 16035–16048

Information) show that the membranes #3S-N and #5S-W can still possess water contact angles of 152.4 ± 0.2° and 151.8 ± 0.3°, respectively at 80 °C. In addition, the superhydrophobicity of #3S-N towards various aqueous liquids at 60, 70, and 80 °C were also examined, as shown in Figure S7 (Supporting Information). The results suggest that the membranes still have superhydrophobic and self-cleaning properties toward these liquids at higher temperatures. Additionally, in order to ensure the FS-SiO_2 stability in the composite membranes during MD testing, these superhydrophobic membranes #3S-N and #5S-W have been eroded by 2 L of NaCl solution with a concentration of 3.5 wt % and a flow rate of 0.6 L min^{-1} for 24 h. After the solutions were scoured for 24 h, the ICP results show that both the original and tested salt solutions contained a negligible amount of Si under the range limit (0.02 ppm of Si for original and tested salt water), which demonstrated that the FS-SiO_2 nanoparticles stay stably in these composite membranes.

As shown in Figure 9A,D, the dual-layer membrane #3S-N has a permeate flux of 24.6 ± 1.2 kg m^{-2} h^{-1}, which is higher than that of #5S-W (20.8 ± 2.8 kg m^{-2} h^{-1}). The flux of the as-prepared membranes are all higher than the commercial GVHP membrane, which only has a flux of 10.6 kg $m^{-2}h^{-1}$ under the same testing conditions.[16] As shown in Figure 9B,E, the surface morphology of the as-developed membranes did not show obvious alteration after continuous MD process while the water contact angles of #3S-N and #5S-W after testing were 152.2 ± 0.4° and 152.6 ± 0.3°, respectively, indicating that the superhydrophobic surface is potentially durable for long-term applications. The cross-sectional images shown in Figure 9C,F prove that the adhesive forces between FS-SiO_2-blended PVDF composite layers and PVDF nanofibrous or PET nonwoven supports are strong enough to avoid any delamination after MD test.

For comparison purpose, PVDF nanofibrous membrane free of silica (thickness =72 ± 4 μm) was also tested in the same MD setup under the same conditions. The properties of the PVDF nanofibrious membrane are listed in Table S1 (Supporting Information) whereas its DCMD performance is shown in Figure S8A (Supporting Information). The PVDF nanofibrious membrane exhibited a lower flux of 15.9 ± 0.9 kg m^{-2} h^{-1}. In addition, the membrane was also wetted fast, within 10 h, as evidenced by the increase in permeate conductivity. The possible reason for the wetting is that the water had strong adhesive force with PVDF nanofibrous surface (Figure S8B, Supporting Information), making it easier to penetrate through the membrane. Once the water penetrates into the membrane, it can accumulate between loose nanofibrous layers (Figure S8C,D, Supporting Information), resulting in a significant decrease of temperature difference and mass transfer rate.[2,36] Therefore, the flux of this membrane is also lower.

Compared with the nanofiber-supported superhydrophobic membrane #3S-N, the nonwoven-supported superhydrophobic membrane #5S-W has a more stable performance over a testing duration of 40 h, even though it has a lower LEPw and larger membrane pore size. This might be attributed to the better wetting resistance of the thicker 3D superhydrophobic structure of membrane #5S-W. Figure 10 schematically illustrates the wetting of the two different superhydrophobic dual-layer membranes, respectively. In the case of the nanofiber-supported membrane (Figure 10A), there is only an ultrathin 3D superhydrophobic layer on the top of the membrane, thus the superhydrophobicity is metastable; once the air or vapor entrapped under the water−membrane interface is lost, wetting of the thin superhydrophobic layer can occur; water could then continuously penetrate the pores of the less hydrophobic PVDF support layer in a relatively faster manner, until completely wetting the membrane. In contrast, as shown in Figure 10B, due to the entire 3D superhydrophobic structure, another stable water−membrane interface with air or vapor entrapped underneath it is immediately created even after the wetting of the topmost layer, which makes the #5S-W a better membrane for long-term MD application. To further optimize the performance of the nonwoven-supported membrane and increase the LEPw without compromising on its strength, further work such as reducing membrane surface pore size is planned.

3.6. Comparison of Properties and DCMD Performance of Different PVDF Nanofiber Membranes. Table 3 compares the properties and DCMD performance of various PVDF nanofiber membranes developed in this work and the literature data. In addition to the high rejection over 99.99%, a flux enhancement of electrospun membrane #3S-N with long stable performance has been achieved in this work, which is attributed to the porous nanofibrous support layer and superhydrophobic skin. The mechanical properties and long-term stability of the nonwoven-supported superhydrophobic dual-layer membrane #5S-W reported in this study are much better than those of other fabricated PVDF nanofiber membrane (stable in continuous testing of 40 h with rejection >99.99%), due to its excellent combination of non-woven support and the unique 3D superhydrophobic structure.

4. CONCLUSIONS

In summary, the structural features of two novel superhydrophobic membranes are very well suited to membrane distillation for the following reasons: (1) the membranes possess contact angles greater than 150°, which means they exhibit superhydrophobicity toward various kinds of liquid such as milk, coffee, juice, and oil-in-water emulsion (1 wt % silica oil in water). The superhydrophobic nature of the membranes makes them suitable for not only water desalination but also concentrating other solutions; (2) the greater hydrophobicity allows membranes with larger pore sizes to be used in the MD process while still maintaining a stable performance in a long-term MD process; (3) the superhydrophobic nanofiber-supported dual-layer membranes have higher porosity that enhances MD flux while the superhydrophobic nonwoven-supported dual-layer membranes exhibit excellent mechanical durability to minimize breakage and also better water intrusion resistance as a result of their thicker 3D micro- and nano-superhydrophobic structure; (4) these superhydrophobic layers are robust and durable in continued MD operations.

To facilitate the application of the electrospun superhydrophobic dual-layer membranes for the water industry, more optimization is needed with respect to controlling membrane maximum pore size and enhancing membrane long-term performance. For example, the antiwetting property of the electrospun membranes could be further improved by reducing the membrane pore size via tuning the PVDF/FS-SiO_2 dope composition, covering an ultrathin nanofibrous skin with thinner fibers without changing surface roughness, or grafting a thin hydrophobic layer onto the membrane surface.

■ ASSOCIATED CONTENT

Supporting Information

Water sliding angle measurement (Figure S1); liquid enter pressure of water (LEPw) test (Figure S2); porosity measurement; schematic drawing of agglomerated silica nanoparticles and modified silica dispersed in PVDF matrix (Figure S3); mechanisms of modification reaction on silica nanoparticles (Figure S4); pore size distribution of different PVDF membranes (Figure S5); temperature dependence of water contact angles (Figure S6); photographs of various liquids on superhydrophobic membrane #3S-N surface and after tilting the membrane (Figure S7); DCMD continuous performance of the PVDF nanofibrous membrane at the feed and permeate temperatures of 60 and 20 °C, the surface morphology and water contact angle image of PVDF nanofiber membrane, and photograph and cross sectional morphology of the PVDF nanofibrous membrane after MD testing (Figure S8); surface properties of PVDF nanofibrous membrane (Table S1). This material is available free of charge via the Internet at http://pubs.acs.org.

■ AUTHOR INFORMATION

Corresponding Author

*R. Wang. Email: rwang@ntu.edu.sg. Tel: (65) 6790-5327. Fax: (65) 6515-5981.

Notes

The authors declare no competing financial interest.

■ ACKNOWLEDGMENTS

This research grant is supported by the Singapore National Research Foundation under its Environmental & Water Technologies Strategic Research Programme and administered by the Environment & Water Industry Programme Office (EWI) of the PUB (EWI RFP 0901-IRIS-02-03). The first author is supported by the National Research Foundation Singapore under its National Research Foundation (NRF) Environmental and Water Technologies (EWT) PhD Scholarship Programme and administered by the Environment and Water Industry Programme Office (EWI). We also acknowledge funding support from the Singapore Economic Development Board to the Singapore Membrane Technology Centre. Insightful comments and suggestions from Professor William B. Krantz are highly appreciated.

■ REFERENCES

(1) Khayet, M. Membranes and Theoretical Modeling of Membrane Distillation: A Review. *Adv. Colloid Interface Sci.* **2011**, *164*, 56−88.

(2) Liao, Y.; Wang, R.; Tian, M.; Qiu, C.; Fane, A. G. Fabrication of Polyvinylidene Fluoride (PVDF) Nanofiber Membranes by Electro-Spinning for Direct Contact Membrane Distillation. *J. Membr. Sci.* **2013**, *425−426*, 30−39.

(3) Yang, X.; Wang, R.; Fane, A. G. Novel Designs for Improving the Performance of Hollow Fiber Membrane Distillation Modules. *J. Membr. Sci.* **2011**, *384*, 52−62.

(4) Yu, H.; Yang, X.; Wang, R.; Fane, A. G. Numerical Simulation of Heat and Mass Transfer in Direct Membrane Distillation in a Hollow Fiber Module with Laminar Flow. *J. Membr. Sci.* **2011**, *384*, 107−116.

(5) Chen, G.; Yang, X.; Wang, R.; Fane, A. G. Performance Enhancement and Scaling Control with Gas Bubbling in Direct Contact Membrane Distillation. *Desalination* **2013**, *308*, 47−55.

(6) Yu, H.; Yang, X.; Wang, R.; Fane, A. G. Analysis of Heat and Mass Transfer by CFD for Performance Enhancement in Direct Contact Membrane Distillation. *J. Membr. Sci.* **2012**, *405−406*, 38−47.

(7) Zuo, G.; Wang, R.; Field, R.; Fane, A. G. Energy Efficiency Evaluation and Economic Analyses of Direct Contact Membrane Distillation System Using Aspen Plus. *Desalination* **2011**, *283*, 237−244.

(8) Manna, A. K.; Sen, M.; Martin, A. R.; Pal, P. Removal of Arsenic from Contaminated Groundwater by Solar-Driven Membrane Distillation. *Environ. Pollut.* **2010**, *158*, 805−811.

(9) Gryta, M.; Tomaszewska, M.; Karakulski, K. Wastewater Treatment by Membrane Distillation. *Desalination* **2006**, *198*, 67−73.

(10) Gryta, M.; Karakulski, K.; Morawski, A. W. Purification of Oily Wastewater by Hybrid UF/MD. *Water Res.* **2001**, *35*, 3665−3669.

(11) Tomaszewska, M.; Gryta, M.; Morawski, A. W. Study on the Concentration of Acids by Membrane Distillation. *J. Membr. Sci.* **1995**, *102*, 113−122.

(12) El-Bourawi, M. S.; Ding, Z.; Ma, R.; Khayet, M. A Framework for Better Understanding Membrane Distillation Separation Process. *J. Membr. Sci.* **2006**, *285*, 4−29.

(13) Celia, E.; Darmanin, T.; Taffin de Givenchy, E.; Amigoni, S.; Guittard, F. Recent Advances in Designing Superhydrophobic Surfaces. *J. Colloid Interface Sci.* **2013**, *402*, 1−18.

(14) Wang, X.; Ding, B.; Yu, J.; Wang, M. Engineering Biomimetic Superhydrophobic Surfaces of Electrospun Nanomaterials. *Nano Today* **2011**, *6*, 510−530.

(15) Ma, Z.; Hong, Y.; Ma, L.; Su, M. Superhydrophobic Membranes with Ordered Arrays of Nanospiked Microchannels for Water Desalination. *Langmuir* **2009**, *25*, 5446−5450.

(16) Liao, Y.; Wang, R.; Fane, A. G. Engineering Superhydrophobic Surface on Poly(vinylidene fluoride) Nanofiber Membranes for Direct Contact Membrane Distillation. *J. Membr. Sci.* **2013**, *440*, 77−87.

(17) Li, X.; Wang, C.; Yang, Y.; Wang, X.; Zhu, M.; Hsiao, B. S. Dual-Biomimetic Superhydrophobic Electrospun Polystyrene Nanofibrous Membranes for Membrane Distillation. *ACS Appl. Mater. Interfaces* **2014**, *6*, 2423−2430.

(18) Feng, L.; Zhang, Y.; Xi, J.; Zhu, Y.; Wang, N.; Xia, F.; Jiang, L. Petal Effect: A Superhydrophobic State with High Adhesive Force. *Langmuir* **2008**, *24*, 4114−4119.

(19) Yohe, S. T.; Freedman, J. D.; Falde, E. J.; Colson, Y. L.; Grinstaff, M. W. A Mechanistic Study of Wetting Superhydrophobic Porous 3D Meshes. *Adv. Funct. Mater.* **2013**, *23*, 3628−3637.

(20) Yohe, S. T.; Herrera, V. L. M.; Colson, Y. L.; Grinstaff, M. W. 3D Superhydrophobic Electrospun Meshes as Reinforcement Materials for Sustained Local Drug Delivery against Colorectal Cancer Cells. *J. Controlled Release* **2012**, *162*, 92−101.

(21) Zhu, Y.; Li, J.; Wan, M.; Jiang, L. Superhydrophobic 3D Microstructures Assembled from 1D Nanofibers of Polyaniline. *Macromol. Rapid Commun.* **2008**, *29*, 239−243.

(22) Li, Y.; Jia, W.-Z.; Song, Y.-Y.; Xia, X.-H. Superhydrophobicity of 3D Porous Copper Films Prepared Using the Hydrogen Bubble Dynamic Template. *Chem. Mater.* **2007**, *19*, 5758−5764.

(23) Wang, K. Y.; Foo, S. W.; Chung, T.-S. Mixed Matrix PVDF Hollow Fiber Membranes with Nanoscale Pores for Desalination through Direct Contact Membrane Distillation. *Ind. Eng. Chem. Res.* **2009**, *48*, 4474−4483.

(24) Wang, P.; Chung, T.-S. Design and Fabrication of Lotus-Root-like Multi-Bore Hollow Fiber Membrane for Direct Contact Membrane Distillation. *J. Membr. Sci.* **2012**, *421−422*, 361−374.

(25) Wang, P.; Chung, T.-S. A New-Generation Asymmetric Multi-Bore Hollow Fiber Membrane for Sustainable Water Production via Vacuum Membrane Distillation. *Environ. Sci. Technol.* **2013**, *47*, 6272−6278.

(26) Zou, H.; Wu, S.; Shen, J. Polymer/Silica Nanocomposites: Preparation, Characterization, Properties, and Applications. *Chem. Rev.* **2008**, *108*, 3893−3957.

(27) Jana, S. C.; Jain, S. Dispersion of Nanofillers in High Performance Polymers Using Reactive Solvents as Processing Aids. *Polymer* **2001**, *42*, 6897−6905.

(28) Kim, H.; Dubois, G. *Dekker Encyclopedia of Nanoscience and Nanotechnology*, 2nd ed; Taylor & Francis Publications; London, 2005.

(29) Wongchitphimon, S.; Wang, R.; Jiraratananon, R. Surface Modification of Polyvinylidene Fluoride-co-Hexafluoropropylene (PVDF−HFP) Hollow Fiber Membrane for Membrane Gas Absorption. *J. Membr. Sci.* **2011**, *381*, 183−191.
(30) Liao, Y.; Wang, Y.; Feng, X.; Wang, W.; Xu, F.; Zhang, L. Antibacterial Surfaces through Dopamine Functionalization and Silver Nanoparticle Immobilization. *Mater. Chem. Phys.* **2010**, *121*, 534−540.
(31) Tang, Z.; Qiu, C.; McCutcheon, J. R.; Yoon, K.; Ma, H.; Fang, D.; Lee, E.; Kopp, C.; Hsiao, B. S.; Chu, B. Design and Fabrication of Electrospun Polyethersulfone Nanofibrous Scaffold for High-Flux Nanofiltration Membranes. *J. Polym. Sci., Part B: Polym. Phys.* **2009**, *47*, 2288−2300.
(32) Cassie, A. B. D.; Baxter, S. Wettability of Porous Surfaces. *Trans. Faraday Soc.* **1944**, *40*, 546−551.
(33) Bhushan, B.; Jung, Y. C. Natural and Biomimetic Artificial Surfaces for Superhydrophobicity, Self-Cleaning, Low Adhesion, and Drag Reduction. *Prog. Mater. Sci.* **2011**, *56*, 1−108.
(34) Schneider, K.; Hölz, W.; Wollbeck, R.; Ripperger, S. Membranes and Modules for Transmembrane Distillation. *J. Membr. Sci.* **1988**, *39*, 25−42.
(35) Lawson, K. W.; Lloyd, D. R. Membrane Distillation. *J. Membr. Sci.* **1997**, *124*, 1−25.
(36) Liao, Y.; Wang, R.; Fane, A. G. Fabrication of Bioinspired Composite Nanofiber Membranes with Robust Superhydrophobicity for Direct Contact Membrane Distillation. *Environ. Sci. Technol.* **2014**, *48*, 6335−6341.
(37) Prince, J. A.; Singh, G.; Rana, D.; Matsuura, T.; Anbharasi, V.; Shanmugasundaram, T. S. Preparation and Characterization of Highly Hydrophobic Poly(vinylidene fluoride)−Clay Nanocomposite Nanofiber Membranes (PVDF−Clay NNMS) for Desalination Using Direct Contact Membrane Distillation. *J. Membr. Sci.* **2012**, *397*−*398*, 80−86.
(38) Lalia, B. S.; Guillen-Burrieza, E.; Arafat, H. A.; Hashaikeh, R. Fabrication and Characterization of Polyvinylidenefluoride-co-Hexafluoropropylene (PVDF-HFP) Electrospun Membranes for Direct Contact Membrane Distillation. *J. Membr. Sci.* **2013**, *428*, 104−115.
(39) Essalhi, M.; Khayet, M. Self-Sustained Webs of Polyvinylidene Fluoride Electrospun Nanofibers at Different Electrospinning Times: 1. Desalination by Direct Contact Membrane Distillation. *J. Membr. Sci.* **2013**, *433*, 167−179.